Journal of Metals, Materials and Minerals, 36(4), e2550, 2026

Effect of anodization voltage and heat treatment on the surface crystallinity and hydrophilicity of the Ti-6Al-4V

Phanawan WHANGDEE[1,*] Peerawat LAOHANA[2], Saranisorn SRIKAM[2], Wittawat SAENRANG[2], Nampueng PANGPAIBOON[3], and Dujreutai PONGKAO KASHIMA[4]

[1] *Department of Applied Physics, Faculty of Sciences and Liberal Arts, Rajamangala University of Technology Isan, Nakhon Ratchasima, 30000, Thailand*
[2] *School of Physics, Institute of Science, Suranaree University of Technology, Nakhon Ratchasima, 30000, Thailand*
[3] *Department of Industrial Physics and Medical Instrumentation, Faculty of Applied Science, King Mongkut's University of Technology North Bangkok, Bangkok, 10800, Thailand*
[4] *Department of Materials Science, Faculty of Science, Chulalongkorn University, Patumwan, Bangkok, 10330, Thailand*

***Corresponding author e-mail**: phanawan.wh@rmuti.ac.th

Received date:
31 October 2025
Revised date:
11 December 2025
Accepted date:
20 March 2026

Keywords:
Hydrophilicity;
Heat treatment;
Crystallinity;
TiO_2

Abstract

The formation of superhydrophilic surfaces on Ti-6Al-4V was achieved through anodization at different voltages, followed by heat treatment at 1000°C for 2 h. This treatment not only enhanced surface crystallinity but also induced morphological changes. A comprehensive analysis of surface properties, including morphology, phase composition, elemental structure, surface roughness, and hydrophilicity, was conducted using OM, FE-SEM, EDX, XRD, AFM, 3D laser scanning confocal microscope, and contact angle measurements, respectively. The TiO_2 anodized films exhibited enhanced crystallinity, increased surface roughness, and a higher oxygen-to-titanium ratio. As a result, the TiO_2 anodized films showed consistent morphology and distribution of elements, with high temperature annealing leading to a transformation from amorphous to crystalline structures, accompanied by elevated surface roughness, and augmented hydrophilicity.

1. Introduction

Ti-6Al-4V is widely used for dental implants because it has outstanding biocompatibility [1–5], great mechanical properties [6–10], and high corrosion resistance [11–15]. However, its bioinert surface makes osseointegration harder [16–20]. Anodization is a very effective way to change the surface of something, although high-voltage methods tend to use a lot of energy and cost a lot [21]. Low-voltage anodization is a safer and cheaper way to do things, but it usually makes amorphous TiO_2 that doesn't work as well. This study employs low-voltage anodization in conjunction with controlled annealing to create crystalline TiO_2 films. This study is unusual in its examination of how voltage-dependent oxide development and subsequent annealing-induced phase transformation affect multiscale surface roughness and hydrophilicity in dental implant applications.

2. Experimental

The titanium alloy (Ti-6Al-4V) sheet was cut to a size of 1 cm × 2 cm × 0.1 cm. It was polished with SiC papers with grit sizes of 280, 400, 600, 1200, and 2000. Then, the sample was cleaned with DI water and etched in a 1 M hydrofluoric acid solution (HF, 48%, Merck, Germany) for one minute. The titanium alloy (Ti-6Al-4V) sheet was used as the working electrode, while the graphite was used as the counter electrode. The TiO_2 anodized film was performed by anodizing in a solution of 1 M phosphoric acid (H_3PO_4, 85%, QRëC, New Zealand) and 80% V/V ethanol (C_2H_5OH, 99.9%, QRëC, New Zealand). The voltage was used between 5 V and 20 V for 80 min. The TiO_2 anodized film was annealed at 1000°C for 2 h after anodization. The TiO_2 anodized films were annealed at 1000°C to achieve a rutile-dominated TiO_2 phase, as annealing at 400°C to 600°C resulted in mixed anatase–rutile structures. This treatment was applied to investigate oxide phase evolution rather than to preserve the Ti-6Al-4V substrate microstructure.

An optical microscope (Leica DM4 optical microscope) was used to examine the color of the film. The surface morphology and elemental content of the TiO_2 anodized film were studied using a Field emission scanning electron microscope (FE-SEM) and energy-dispersive X-ray spectroscopy (EDX) (Carl Zeiss Auria, Germany). Atomic force microscopy (AFM) (XE-120 Park System, Korea) was employed to evaluate nanoscale surface roughness of the TiO_2 anodized films. After annealing, the surface topography became significantly rougher with pronounced microscale features, exceeding the reliable vertical and lateral measurement limits of AFM. Therefore, the roughness of the TiO_2 anodized films after annealing was characterized by using a 3D laser scanning confocal microscope (Olympus LEXT OLS5100),

which allows quantitative assessment of microscale roughness over a larger sampling area. The crystalline structure of the TiO_2 anodized film was investigated by using X-ray diffraction (XRD) with a Bruker D2 Phaser. The water contact angle was determined using the contact angle measuring method.

3. Results and discussion

3.1 Anodization potential control

Figure 1 shows the current-time curves comparison of anodization of Ti-6Al-4V at different voltages of 5 V, 10 V, 15 V, and 20 V. Within the initial few seconds of the anodization process, the current suddenly increases to a maximum value before rapidly decreasing. This behavior corresponds to the formation of a thin TiO_2 layer on the Ti-6Al-4V surface, which slowly increases the electrical resistance due to decreasing ion transport. During the anodization process, the current continually maintains a stable level, indicating the formation of a dynamic equilibrium between the oxide's growth and its dissolution. The initial current density increases with the increasing applied voltage, indicating that higher current density enhances ionic migration and promotes oxide formation [22–27]. The 20 V condition exhibited the highest initial current, approximately 2000 μA, in comparison to other voltages, indicating a faster oxide growth and thicker films. In contrast, the 5 V curve exhibits the lowest and most stable current, suggesting the formation of a thinner oxide layer. An increasing current during extended anodization at elevated voltages (≥ 10 V) may result from localized dielectric breakdown within the oxide, thereby improving ionic conduction through the film.

3.2 The structural color formation of TiO_2 anodized films

The optical microscope images of the TiO_2 anodized films (Figure 2) show a shift in interference colors of TiO_2 anodized films, from bright yellow at 5 V to blue at 20 V. The color progression from yellow (5V) to deep yellow (10V), orange/gold (15V), and blue (20 V) is caused by thin-film interference in the TiO_2 anodized layers. Coloration is determined by Fresnel reflections at the air/ TiO_2 and TiO_2/Ti-6Al-4V interfaces. Constructive interference occurs when the optical path difference satisfies $2^{nd} = m\lambda$, where n is TiO_2's refractive index and d is the oxide thickness. Increasing anodization voltage promotes field-assisted ionic migration, resulting in a progressive increase in oxide thickness [28–30]. This thickness increase causes a systematic shift in the interference state, shifting the dominant reflected wavelengths within the visible spectrum. As a result, the interference maxima travel across different spectral regions in a nonlinear yet periodic manner, producing the observed color pattern. This behavior is related to the current-time curves, as shown in Figure 1. These curves indicated that increasing applied voltages resulted in higher starting currents and a slower decay to steady-state, which implies that oxide development and thickening occurred more rapidly. As can be seen in Figure 2(e), the appearance of color on the TiO_2 anodized films may be explained by the coherent reflection of visible wavelengths that occurs as a result of interference between TiO_2 anodized films and layers of Ti-6Al-4V [31–33]. This phenomenon allows for the formation of color.

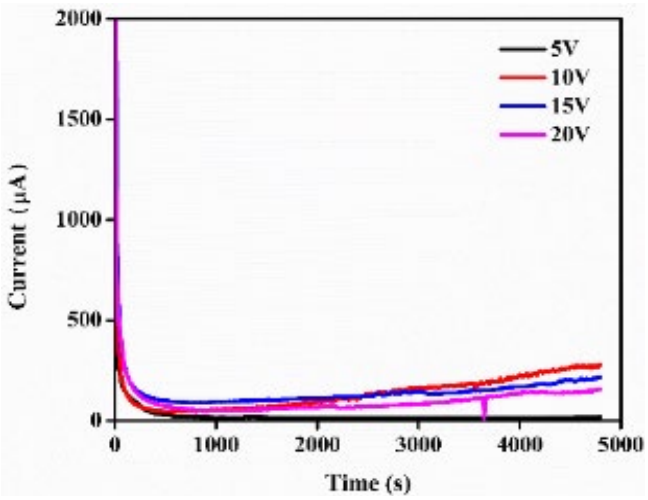

Figure 1. Current-time curves comparison of anodization of Ti-6Al-4V at different voltages of 5 V, 10 V, 15 V, and 20 V.

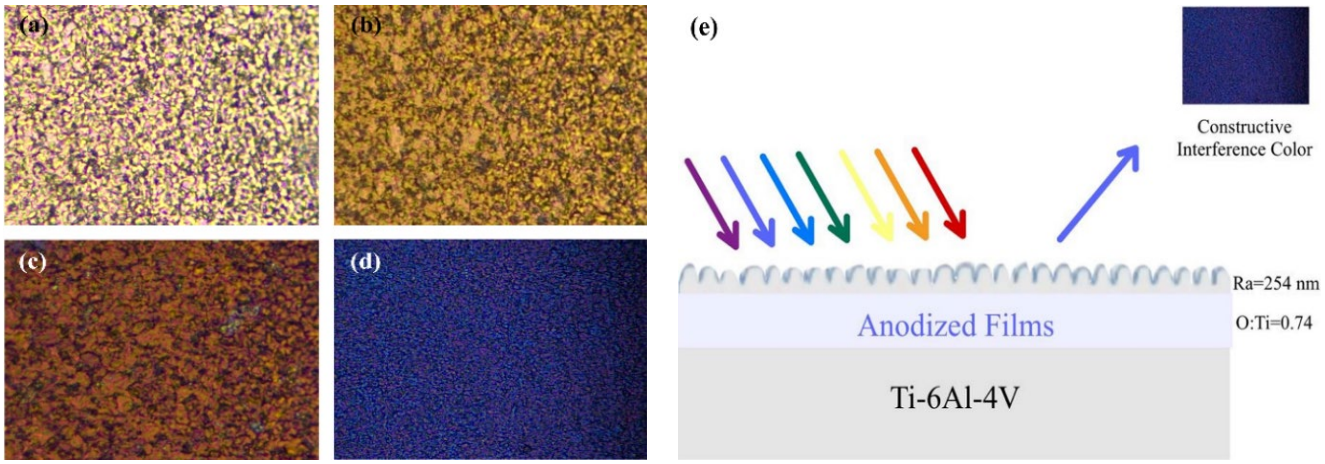

Figure 2. Optical microscope images of the TiO_2 anodized films formed at (a) 5 V, (b) 10 V, (c) 15 V, (d) 20 V, and (e) Schematic presentation of the structural color formation on the TiO_2 anodized films (20 V).

3.3 Surface morphology and structure of TiO_2 anodized films before and after the annealing process

FE-SEM images of the TiO_2 anodized films at different voltages (5 V to 20 V), both before (a–d) and after (e–h) annealing, as shown in Figure 3. The results suggest that the surface morphology before annealing depended on the applied voltage. At 5 V before annealing (Figure 3(a)), the surface morphology is elongated plate-like structures and parallel ridges with the absence of a well-developed porous oxide structure. The TiO_2 anodized films formed at 10 V (Figure 3(b)) showed a granular structure with slightly more thickness and homogeneity. The TiO_2 anodized film formed at 15 V (Figure 3(c)) is porous because ionic transport and oxide dissolution are improved after anodization. At 20 V before annealing (Figure 3(d)), the surface appears relatively smooth and exhibits continuous, parallel features without clearly defined pores. This morphology indicates the formation of a uniformly covering anodic oxide layer under high anodization voltage.

After annealing (Figure 3(e–h)), significant microstructural evolution was observed. The TiO_2 anodized films formed at 5 V (Figure 3(e)) revealed the formation of small crystalline grains, likely rutile TiO_2. The TiO_2 anodized films formed at 10 V (Figure 3(f)) show well-formed plate- and rod-shaped crystals emerged due to the crystallization of the amorphous film into the rutile phase. The TiO_2 anodized films formed at 15 V after annealing (Figure 3(g)) exhibit a uniformly crystallized surface morphology. Annealing promotes homogeneous densification, resulting in a smoother microscale surface relative to other annealed conditions. In contrast, the TiO_2 anodized films formed at 20 V after annealing (Figure 3(h)) display a highly irregular pattern with non-uniform grain growth. Therefore, the morphological transition from a smooth, amorphous oxide (before annealing) to a dense, crystalline structure (after annealing) reflects the combined influence of anodization voltage and annealing.

Figure 4 displays AFM topography images of the TiO_2 anodized films formed at (a) 5 V, (b) 10 V, (c) 15 V, and (d) 20 V before the annealing process. The surface morphology exhibits a distinct progression in nanoscale roughness as anodizing voltage increases. At 5 V, the TiO_2 anodized film displays a rather smooth texture characterized by tiny, uniformly dispersed nodules (R_a = 196 nm). As the voltage rises to 10 V and 15 V, the TiO_2 anodized film surface exhibits a considerable increase in roughness, evidenced by elevated and more irregular peaks and valleys (R_a = 221 nm and 239 nm, respectively). The maximum roughness occurs at 20V (R_a = 254 nm), characterized by distinct granular characteristics and deeper troughs. The increase in R_a with higher applied voltage indicates a strong relationship between the electric field strength and the amount of oxide formed. As the applied voltage increases, ionic migration and oxide formation increase. This results in surfaces that are coarser and denser. The rise in nanoscale roughness corresponds to the current-time curve (Figure 1), which means that the oxide was formed faster and the starting currents were higher at high voltage. In biomedical applications, rougher surfaces may be better for cell adhesion and osseointegration because they could make the surface more hydrophilic and increase its surface energy [21].

The 3D laser scanning confocal microscope images of the TiO_2 anodized films formed at (a) 5 V, (b) 10 V, (c) 15 V, and (d) 20 V after the annealing process are shown in Figure 5. The surface roughness (R_a) reveals a small change with voltage, occurring between the range of 6 µm to 8 µm. The TiO_2 anodized films formed at 15 V demonstrate the lowest roughness (~6.4 µm), while the TiO_2 anodized films formed at 10 V demonstrate the maximum roughness (~7.6 µm).

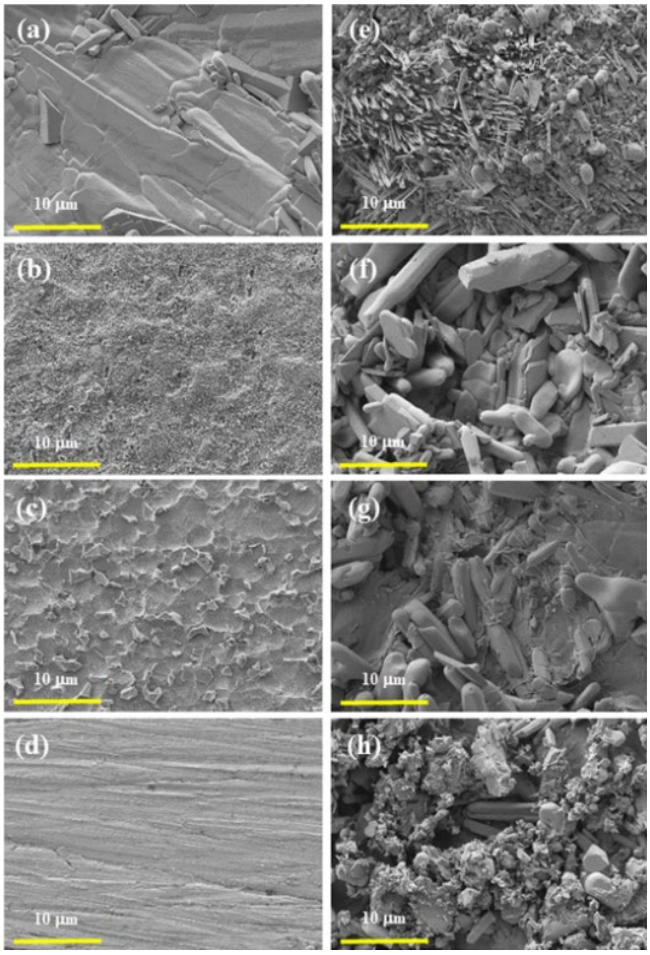

Figure 3. FE-SEM images of the TiO_2 anodized films formed at (a) 5, (b) 10, (c) 15 and (d) 20V before and after the annealing process (e-h).

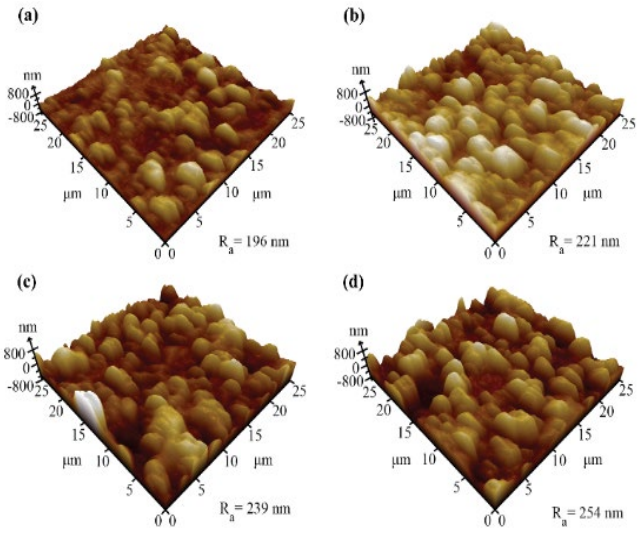

Figure 4. AFM topography images of the TiO_2 anodized films formed at (a) 5 V, (b) 10 V, (c) 15 V, and (d) 20 V before the annealing process.

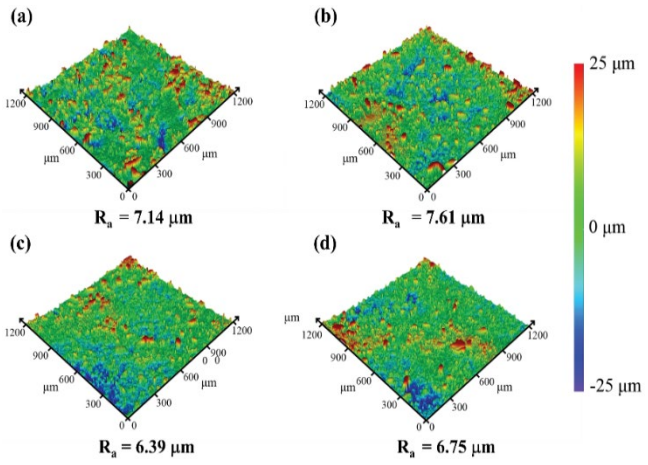

Figure 5. 3D laser scanning confocal microscope images of the TiO_2 anodized films formed at (a) 5 V, (b) 10 V, (c) 15 V, and (d) 20V after the annealing process.

The significant difference between AFM roughness values ($R_a \approx$ 0.20 µm to 0.25 µm) and those obtained from 3D confocal microscopy ($R_a \approx$ 6 µm to 8 µm) is primarily due to differences in scale and area of measurement. AFM reflects nanoscale surface roughness within a confined area, while 3D confocal microscopy is more sensitive to changes in height at the microscale and thus shows the overall surface morphology. After annealing, surface roughness is mainly controlled by thermal rearrangement, which is directly related to the thickness and initial uniformity of the TiO_2 anodized film. The TiO_2 anodized films formed at 15 V exhibited the most continuous and uniform roughness distribution, resulting in uniform compaction and crystallization of TiO_2 after annealing, leading to a decrease in microscale roughness. Conversely, the TiO_2 anodized films formed at 20 V resulted in a coarser oxide layer, leading to non-homogeneous crystallization and uneven grain growth after annealing, which increased roughness.

3.4 XRD and EDX of TiO_2 anodized films before and after the annealing process

In the as-anodized condition (Figure 6(a)), the only peaks detected were those of the Ti substrate, namely α-Ti (JCPDS card no. 44-1294) and β-Ti (JCPDS card no. 44-1288) [34,35], suggesting that the oxide layers formed at 5 V to 20 V were amorphous [36,37]. The crystallization of the amorphous oxide into rutile was confirmed by the distinct peaks corresponding to the rutile TiO_2 phase (JCPDS card no. 21-1276) [38] at $2\theta \approx 27.48°$, 36.16°, 41.36°, 54.52°, and 56.64° after annealing (Figure 6(b)), indicating the presence of the rutile crystal planes (110), (101), (111), (211), and (220), respectively [2,7,12,21,31,36-48]. The intensity of rutile peaks increased as the anodizing voltage increased, particularly at 15 V and 20 V. This result indicates that higher voltages promoted the formation of denser oxide layers, which simplified phase transformation during the annealing process. The morphological evolution observed by FE-SEM (Figure 3), which revealed dense rod- and plate-like crystal structures after annealing, and by 3D laser scanning confocal microscope (Figure 5), which demonstrated increased roughness associated with grain growth, is consistent with this crystallization behavior.

Annealing at 1000°C produced a predominantly rutile TiO_2 film, whereas annealing at 400°C to 600°C produced mixed anatase–rutile phases. Partial film detachment was observed after high temperature annealing due to thermally induced interfacial stress, although catastrophic spallation did not occur. Therefore, annealing at 1000°C is not proposed as a practical processing route for biomedical implants but was employed to elucidate TiO_2 phase evolution and adhesion trade-offs. Lower annealing temperatures may be more appropriate for clinical applications.

The EDX-mapping analysis, as shown in Figure 7-8, indicated the compositional changes in the TiO_2 anodized films before and after the annealing procedure. As the applied voltage increased from 5 V to 20 V, the oxygen content progressively increased from 16% to 39% prior to annealing, while the titanium content decreased from 72% to 52%. This suggests that the formation of a thicker, oxygen-rich oxide layer is facilitated by higher anodization voltages, which also promote increased oxidation [21]. The minor quantities of aluminum and vanadium have been detected in all conditions [7-9,11]. This indicates that these alloying elements have partially diffused near the oxide–metal interface.

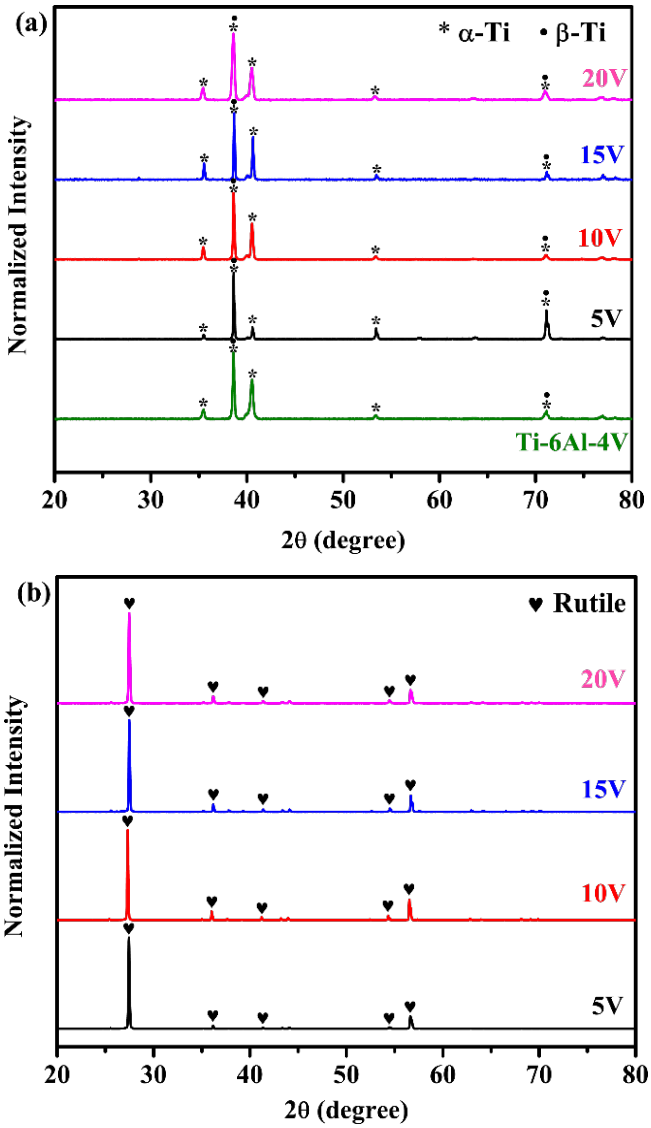

Figure 6. Normalized XRD patterns of TiO_2 anodized films coated on Ti-6Al-4V substrates modified with 4 different conditions (5 V, 10 V, 15 V, and 20 V) (a) before, and (b) after the annealing process.

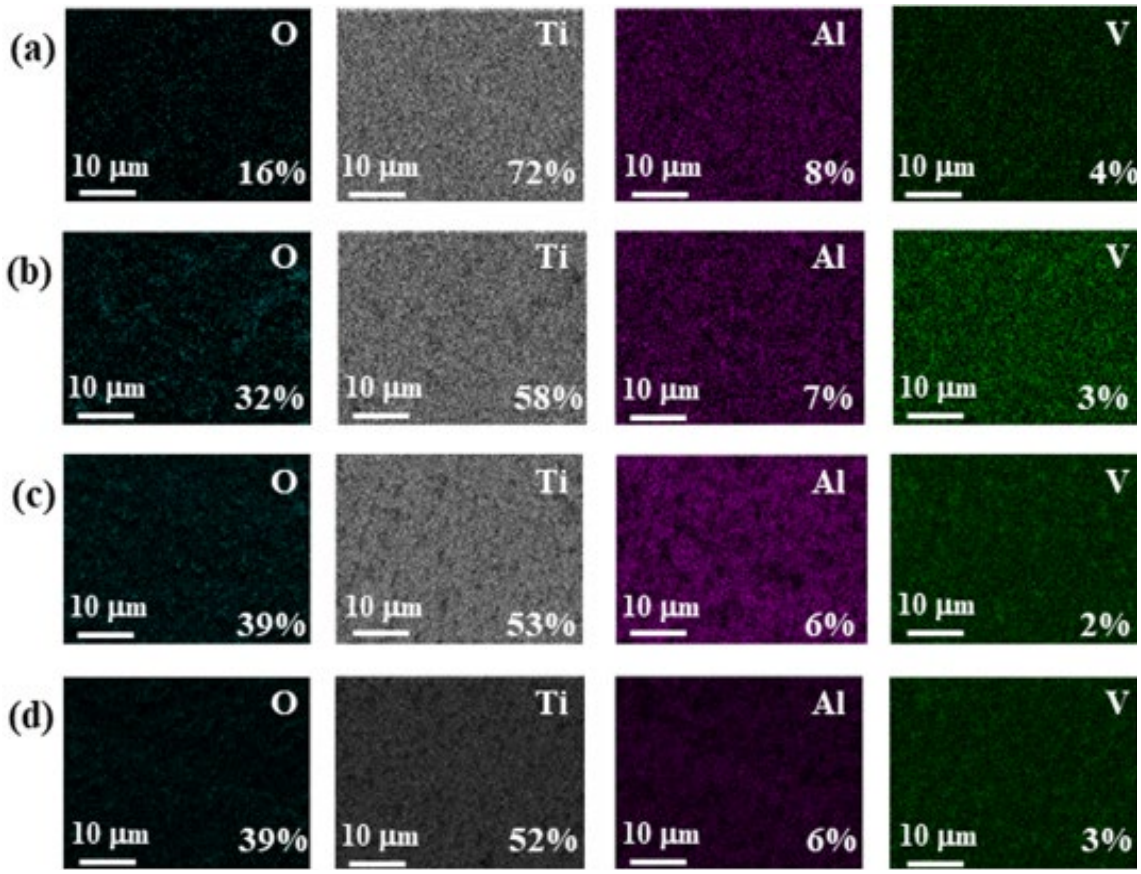

Figure 7. EDX-mapping analysis images of the TiO_2 anodized films formed at (a) 5 V, (b) 10 V, (c) 15 V, and (d) 20 V before the annealing process.

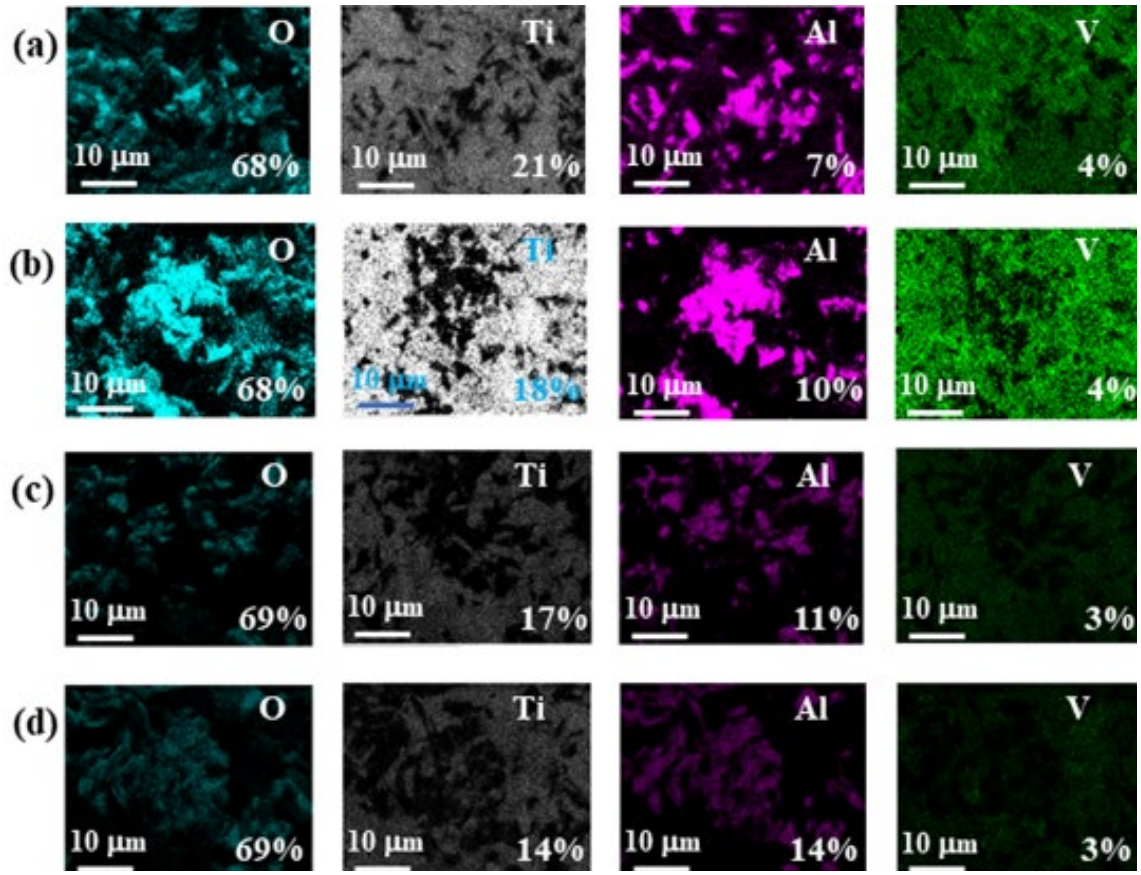

Figure 8. EDX-mapping analysis images of the TiO_2 anodized films formed at (a) 5 V, (b) 10 V, (c) 15 V, and (d) 20 V after the annealing process.

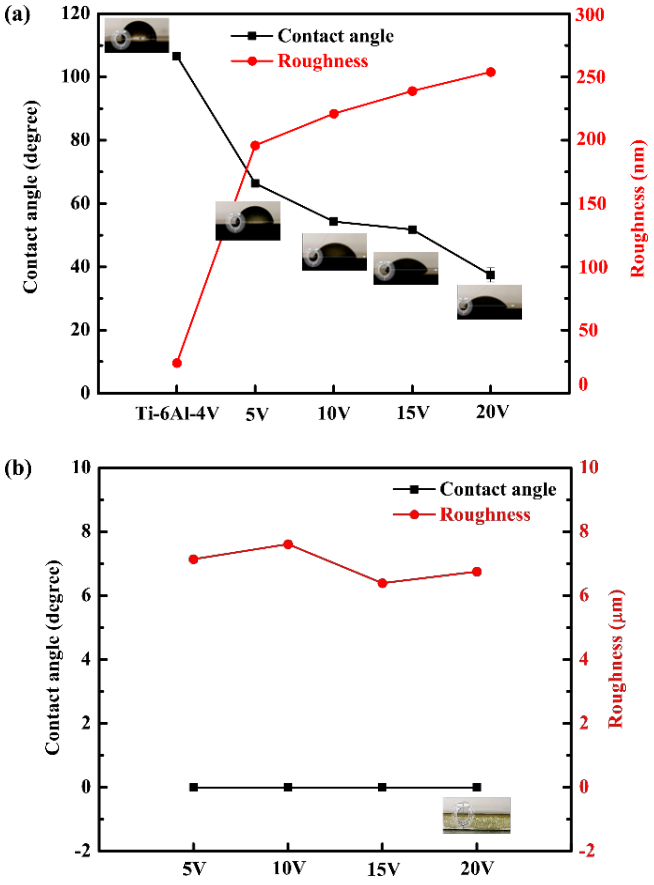

Figure 9. The contact angle and roughness of the TiO_2 anodized films at different voltages of 5 V, 10 V, 15 V, and 20 V, (a) before, and (b) after the annealing process.

The EDX shift after annealing (O increasing to 68% to 69% with a decrease in Ti to 14% to 21%) is consistent with thermally enhanced oxidation and oxygen inward diffusion. Because EDX is not phase-selective and probes a finite depth, a thicker, more oxygen-rich TiO_2 layer will bias the measured composition toward higher O and lower metallic Ti [21,49]. Regarding Al and V, high-temperature exposure can promote element redistribution, such as Al (high oxygen affinity) being enriched in the near-surface oxide/suboxide region, while V tends to be comparatively depleted or segregated depending on local oxidation kinetics. These compositional changes correspond to the structural transformation observed in the XRD patterns (Figure 6), which resulted in the conversion of amorphous films to crystalline rutile TiO_2 after annealing.

3.5 Hydrophilic properties of TiO_2 anodized films before and after the annealing process

Figure 9 illustrates the correlation between the hydrophilicity and surface roughness of the TiO_2 anodized films before and after annealing. The TiO_2 anodized films demonstrated a distinct trend from approximately 196 nm (5 V) to approximately 254 nm (20 V) in surface roughness before annealing (Figure 9(a)), as corroborated by AFM analysis (Figure 4). The increase in surface roughness enhances hydrophilicity due to the Wenzel effect. The contact angle gradually decreased from approximately 66° at 5V to around 37° at 20V as the nanoscale roughness increased.

All TiO_2 anodized films exhibited a near-zero contact angle after annealing (Figure 9(b)), which suggests that superhydrophilicity was independent of the applied voltage. The crystallization of the amorphous oxide into rutile, as demonstrated by XRD results (Figure 6(b)), and the increased oxygen content on the surface, as confirmed by EDX mapping (Figure 8), are the likely causes of this significant transformation. The surface was primarily driven toward superhydrophilicity by the combination of rutile crystallinity, oxygen enrichment, and nanoscale topography [45,50-53]. However, the microscale roughness measured by 3D laser scanning confocal microscope (Figure 5) revealed only minimal differences among the voltages. These results indicate that anodization could enhance roughness, resulting in hydrophilicity, whereas annealing directs phase transformation and surface chemistry, resulting in the production of stable superhydrophilic TiO_2 films that are highly desirable for biomedical applications, including protein adsorption and osteoblast adhesion [8,11,13,36,40,54].

4. Conclusions

The TiO_2 anodized films were performed on the Ti-6Al-4V alloy using low voltage, followed by annealing. The current-time profiles and color evolution seen using optical microscopy indicate that the applied voltage significantly influenced the oxide growth rate, thickness, and surface morphology. The increased voltage resulting in an increase in surface roughness was demonstrated by AFM and 3D laser scanning confocal microscope analyses, while oxygen enrichment was confirmed by EDX. The amorphous oxide significantly transformed into rutile TiO_2 after annealing, as evidenced by XRD. This change was accompanied by an elevation in oxygen content at the surface. The combination of surface roughness and structural crystallization resulted in a significant enhancement of hydrophilicity. The contact angle went from 66° in the as-anodized films to about 0° after annealing. This made the films superhydrophilicity, no matter what the anodizing voltage was. This change results from the combinatorial actions of nanoscale roughness and rutile phase development. The resulting TiO_2 anodized films are expected to enhance surface bioactivity significantly, particularly regarding protein adsorption and osteoblast adhesion, highlighting their substantial potential for dental and orthopedic implant applications.

Acknowledgements

The authors would like to thank Miss Weeraya Drechsler, Miss Natthaphorn Haochatturat, and Mr. Thiwat Sunthamala for helping us. This research project is supported by Science Research and Innovation Fund. Agreement No. FF68/NKR/037.

References

[1] Z. Wang, W. Huang, and X. Meng, "Electrochemical behaviour of Ti–25Nb–3Mo–3Zr–2Sn biomedical alloy in different simulated physiological environments," *Materials Science and Technology*, vol. 31, pp. 1335–1341, 2015.

[2] S. Boonrungsiman, P. Prompinit, P. Khemthong, T. Wutikhun, A. Treethong, P. Kasamechonchung, N. Chanlek, R. Maniratanachote, M. Horprathum, A. Pankiew, S. Pornthreeraphat, N. Khemasiri, and A. Klamchuen, "Effects of thermal treatment on hydrophilicity and corrosion resistance of Ti surface," *Surface and Interface Analysis*, vol. 51, no. 3, pp. 308–315, 2019.

[3] P. Whangdee, W. Saenrang, and D. Pongkao Kashima, "Effect of fluoride and hydroxyl group on bioactivity of the anodized films prepared by two-step anodization at low current density," *Surface and Interface Analysis*, vol. 54, no. 7, pp. 724–733, 2022.

[4] P. Whangdee, S. Nilmoung, N. Pangpaiboon, and D. Pongkao Kashima, "The effect of low current density on the hydrophilicity and surface properties of the anodized films performed by two-step anodization," *SNRU Journal of Science and Technology*, vol. 11, pp. 45–54, 2019.

[5] P. Whangdee, S. Nilmoung, N. Pangpaiboon, and D. Pongkao Kashima, "Effect of ethanol on hydrophilicity of the anodized films performed by two-step anodization at low current density," *Journal of Metals, Materials and Minerals*, vol. 29, no. 3, pp. 60–65, 2019.

[6] Y. M. Wang, B. L. Jiang, L. X. Guo, and T. C. Lei, "Controlled synthesis of microarc oxidation coating on Ti6Al4V alloy and its antifriction properties," *Materials Science and Technology*, vol. 20, no. 12, pp. 1590–1594, 2004.

[7] X.-m. Wang, and F.-q. Zhang, "Influence of anions in phosphate and tetraborate electrolytes on growth kinetics of microarc oxidation coatings on Ti_6Al_4V alloy," *Transactions of Nonferrous Metals Society of China*, vol. 32, pp. 2243–2252, 2022.

[8] P. K. Srivas, K. Kapat, B. Das, P. Pal, P. G. Ray, and S. Dhara, "Hierarchical surface morphology on Ti6Al4V via patterning and hydrothermal treatment towards improving cellular response," *Applied Surface Science*, vol. 478, pp. 806–817, 2019.

[9] C. Wang, H. Huang, Z. Zhang, L. Zhang, J. Yan, and L. Ren, "Formation, evolution and characterization of nanoporous structures on the Ti6Al4V surface induced by nanosecond pulse laser irradiation," *Materials & Design*, vol. 223, p. 111243, 2022.

[10] Y. Xu, Y. Lu, J. Liang, and R. D. Sison, "Microstructure and corrosion behaviour of additively manufactured Ti–6Al–4V with various post-heat treatments," *Materials Science and Technology*, vol. 35, pp. 89–97, 2019.

[11] X. Zhang, Y. Wan, Z. Liu, H. Wang, M. Yu, A. Liu, and D. Zhang, "Preparation and bioactive response of super-hydrophilic surface on selective laser melting titanium," *Procedia CIRP*, vol. 89, pp. 222–227, 2020.

[12] M. Fazel, H. R. Salimijazi, M. Shamanian, M. Minneboo,K. Modaresifar, I. A. J. van Hengel, L. E. Fratila-Apachitei, I. Apachitei, and A. A. Zadpoor, "Osteogenic and antibacterial surfaces on additively manufactured porous Ti-6Al-4V implants: Combining silver nanoparticles with hydrothermally synthesized HA nanocrystals," *Materials Science and Engineering: C*, vol. 120, p. 111745, 2021.

[13] K. H. Cheung, M. B. Pabbruwe, W.-F. Chen, P. Koshy, and C. C. Sorrell, "Effects of substrate preparation on TiO_2 morphology and topography during anodization of biomedical Ti6Al4V," *Materials Chemistry and Physics*, vol. 252, p. 123224, 2020.

[14] A. Vadiraj, M. Kamaraj, U. K. Mudali, and A. K. Nath, "Effect of surface modified layers on fretting fatigue damage of biomedical titanium alloys," *Materials Science and Technology*, vol. 22, no. 9, pp. 1119–1125, 2006.

[15] Y. H. Wong, M. G. Affendy, S. K. Lau, P. C. The, H. J. Lee, C. Y. Tan, and S. Ramesh, "Effects of anodisation parameters on thin film properties: A review," *Materials Science and Technology*, vol. 33, pp. 699–711, 2017.

[16] P. Whangdee, W. Saenrang, and D. Pongkao Kashima, "Effect of surface fluorination on the hydrophilicity of the anodised films for dental implant applications," *Materials Research Innovations*, vol. 24, no. 6, pp. 321–325, 2020.

[17] P. Whangdee, S. Sriprasertsuk, V. Sirmaneepong, and D. Pongkao Kashima, "Surface characteristics and hydrophilicity of the as-anodized films formed at high current density on Ti-6Al-4V in different electrolytes," *Key Engineering Materials*, vol. 608, pp. 274–279, 2014.

[18] P. Whangdee, S. Chukasorn, V. Srimaneepong, T, Watanabe, and D. Pongkao Kashima, "Effects of surface roughness and chemical species on hydrophilicity of anodized film on Ti-6Al-4V formed at a low current density," *Advanced Materials Research*, vol. 664, pp. 774–779, 2013.

[19] V. V. Akimov, E. A. Tyukhai, V. L. Tauson, A. Y. Safronov, A. V. Kashevskii, B. G. Pushkarev, S. B. Nikiforov, and E. V. Voloshin, "Characteristics of morphology, structure and composition of titanium surface under its modification by electrochemical polarization in phosphate-alkaline solutions," *Surface and Interface Analysis*, vol. 47, no. 12, pp. 1081–1097, 2015.

[20] P. Ausiello, E. Bolli, S. Kaciulis, A. Gloria, A. Lanzotti, M. Martorelli, A. Mezzi, R. Montanari, M. Richetta, and A. Varone, "Morphology and microchemistry study of three commercial dental implants," *Surface and Interface Analysis*, vol. 55, no. 5, pp. 411–416, 2023.

[21] S. Durdu, G. Cihan, E. Yalcin, and A. Altinkok, "Characterization and mechanical properties of TiO_2 nanotubes formed on titanium by anodic oxidation," *Ceramics International*, vol. 47, no. 8, pp. 10972–10979, 2021.

[22] X. Li, C. Li, T. Gong, J. Su, W. Zhang, Y. Song, and X. Zhu, "Comparative study on the anodizing process of Ti and Zr and oxide morphology," *Ceramics International*, vol. 47, no. 16, pp. 23332–23337, 2021.

[23] Y. Ni, J. Zhang, T. Gong, M. Sun, Z. Zhao, X. Li, H. Yu, and X. Zhu, "Quantitative analysis of the volume expansion of nanotubes during constant voltage anodization," *Surfaces and Interfaces*, vol. 26, p. 101419, 2021.

[24] C. C. Manole, and C. Pirvu, "Surface and electrochemical analysis for the understanding of TiO_2 nanopores/nanotubes changes in post-elaboration treatment," *Surface and Interface Analysis*, vol. 43, pp. 1022–1029, 2011.

[25] X. Hou, P. D. Lung, and Y. Li, "Controlling anodization time to monitor film thickness, phase composition and crystal orientation during anodic growth of TiO_2 nanotubes," *Electrochemistry Communications*, vol. 134, p. 107168, 2022.

[26] Q. Zhou, M. Tian, Z. Ying, Y. Dan, F. Tang, J. Zhang, J. Zhu, and X. Zhu, "Dense films formed during Ti anodization in NH_4F electrolyte: Evidence against the field-assisted dissolution reactions of fluoride ions," *Electrochemistry Communications*, vol. 111, p. 106663, 2020.

[27] Y. Li, Y. Tan, K. Liang, L. Zhang, and S. Zhang, "Study of the dimensions and photoelectric properties of TiO_2 NTs prepared by the double Ti-Electrode oxidation method," *Journal of Alloys and Compounds*, vol. 859, p. 157878, 2021.

[28] L. Skowronski, and M. Chorobinski, "The effect of thickness and optical constants of the dielectric layer on the color behaviour of the glass/Ti/TiO_2 decorative coatings," *Thin Solid Films*, vol. 691, p. 137595, 2019.

[29] S. Kim, M. Jung, M. Kim, and J. Choi, "Bi-functional anodic TiO_2 oxide: Nanotubes for wettability control and barrier oxide for uniform coloring," *Applied Surface Science*, vol. 407, pp. 353–360, 2017.

[30] A. G. Sanchez, W. Schreiner, G. Duffo, and S. Cere, "Surface modification of titanium by anodic oxidation in phosphoric acid at low potentials. Part 1. Structure, electronic properties and thickness of the anodic films," *Surface and Interface Analysis*, vol. 45, no. 6, pp. 1037–1046, 2013.

[31] O. Yilmaz, M. F. Ebeoglugil, R. Dalmis, and T. Dikici, "Effect of anodizing time on the structural color and photocatalytic properties of the TiO_2 films formed by electrochemical method," *Materials Science in Semiconductor Processing*, vol. 167, p. 107768, 2023.

[32] A. Maciej, A. Wadas, M. Sowa, R. Socha, M. Kubiczek, and W. Simka, "Colourful thin passive films on a Zn-Co alloy formed by anodic oxidation," *Electrochimica Acta*, vol. 373, p. 137922, 2021.

[33] L. Mohan, C. Dennis, N. Padmapriya, C. Anandan, and N. Rajendran, "Effect of electrolyte temperature and anodization time on formation of TiO_2 nanotubes for biomedical applications," *Materials Today Communications*, vol. 23, p. 101103, 2020.

[34] L. Zhang, M. Shao, Z. Zhang, X. Yi, J. Yan, Z. Zhou, D. Fang, Y. He, and Y. Li, "Corrosion behavior of nitrided layer of Ti_6Al_4V titanium alloy by hollow cathodic plasma source nitriding," *Materials,* vol. 16, no. 8, p. 2961, 2023.

[35] M. D. Wadge, M. J. Carrington, H. Constantin, K. Orange, J. Greaves, Md. T. Islam, K. M. Z. Hossain, T. P. Copper, Z. R. Kudrynskyi, R. M. Felfel, I. Ahmed, and D. M. Grant, "Characterization of potential nanoporous sodium titanate film formation on Ti_6Al_4V and TiO_2 microspherical substrates via wet-chemical alkaline conversion," *Materials Characterization,* vol. 185, p. 111760, 2022.

[36] M. Wang, Y. Wu, S. Lu, T. Chen, Y. Zhao, H. Chen, and Z. Tang, "Fabrication and characterization of selective laser melting printed Ti–6Al–4V alloys subjected to heat treatment for customized implants design," *Progress in Natural Science: Materials International*, vol. 26, no. 6, pp. 671–677, 2016.

[37] E. Ahounbar, S. M. M. Khoei, M. Urgen, and M. Shokouhimehr, "Characteristics of the hierarchical porous TiO_2 layer synthesized on Ti via plasma electrolytic oxidation: Role of the applied voltage," *Ceramics International*, vol. 47, no. 6, pp. 8279–8289, 2021.

[38] D. Yang, *Titanium Dioxide - Material for a Sustainable Environment*, London: IntechOpen., 2018, pages 518.

[39] M. Jahdi, S. B. Mishra, E. N. Nxumalo, S. D. Mhlanga, and A. K. Mishra, "Synergistic effects of sodium fluoride (NaF) on the crystallinity and band gap of Fe-doped TiO_2 developed via microwave-assisted hydrothermal treatment," *Optical Materials*, vol. 104, p. 109844, 2020.

[40] M. Fazel, H. R. Salimijazi, M. Shamanian, I. Apachitei, and A. A. Zadpoor, "Influence of hydrothermal treatment on the surface characteristics and electrochemical behavior of Ti-6Al-4V bio-functionalized through plasma electrolytic oxidation," *Surface and Coatings Technology*, vol. 374, pp. 222–231, 2019.

[41] M. Daniyal, S. Akhtar, and A. Azam, "Effect of nano-TiO_2 on the properties of cementitious composites under different exposure environments," *Journal of Materials Research and Technology*, vol. 8, no. 6, pp. 6158–6172, 2019.

[42] S. S. Lephuthing, A. M. Okoro, O. O. Ige, and P. A. Olunambi, "Microstructural and electrochemical studies of spark plasma sintered multiwall carbon nanotubes reinforced TiO_2–MnO_2 based composite," *Journal of Materials Research and Technology*, vol. 12, pp. 894–903, 2021.

[43] A. Medvids, S. Varnagiris, E. Letko, D. Milcius, L. Grase, S. Gaidukovs, A. Mychko, A. Pludons, P. Onufrijevs, and H. Minura, "Phase transformation from rutile to anatase with oxygen ion dose in the TiO_2 layer formed on a Ti substrate," *Materials Science in Semiconductor Processing*, vol. 106, p. 104776, 2020.

[44] T. Kobayashi, and S. Konishi, "Acceleration of wettability switching on TiO_2 thin films under ultraviolet irradiation and direct current bias voltage," *Surface and Coatings Technology*, vol. 363, pp. 80–86, 2019.

[45] F. Meng, L. Xiao, and Z. Sun, "Thermo-induced hydrophilicity of nano-TiO_2 thin films prepared by RF magnetron sputtering," *Journal of Alloys and Compounds*, vol. 485, no. 1–2. pp. 848–852, 2009.

[46] Y. Jiang, H. Liu, K. Shi, C. Tang, and J. Song, "Effect of annealing temperature on wettability of TiO_2/PDA thin films," *Surface and Coatings Technology*, vol. 411, p. 126994, 2021.

[47] O. Secundino-Sánchez, J. Diaz-Reyes, J. Aguila-Lopez, and J. F. Sanchez-Ramirez, "Crystalline phase transformation of electrospinning TiO_2 nanofibres carried out by high temperature annealing," *Journal of Molecular Structure*, vol. 1194, pp. 163–170, 2019.

[48] D. Nesheva, T. Babeva, M. Vasileva, B. Valdez-Salas, V. Dzhurkov, M. U. Grujić-Brojčin, M. J. Šćepanović, O. Perez, N. Nedev, M Curiel, T. Srećković, "Phase characterization and ethanol adsorption in TiO_2 nanotubes anodically grown on Ti6Al4V alloy substrates," *Journal of Alloys and Compounds*, vol. 798, pp. 394–402, 2019.

[49] F. Güzelçimen, F. Güzelçimen, B. Tanören, Ç. Çetinkaya, M. D. Kaya, H. İ. Efkere, Y. Özen, D. Bingöl, M. Sirkeci, B. Kınacı, M. B. Ünlü, S. Özçelik, "The effect of thickness on surface structure of rf sputtered TiO_2 thin films by XPS, SEM/EDS, AFM and SAM," *Vacuum*, vol. 182, p. 109766, 2020.

[50] Y. Jiang, K. Shi, H. Tang, and Y. Wang, "Enhanced wettability and wear resistance on TiO_2/PDA thin films prepared by sol-gel dip coating," *Surface and Coatings Technology*, vol. 375, pp. 334–340, 2019.

[51] R. Sun, Z. Chen, J. Peng, and T. Zheng, "The effect mechanisms of pH, complexant and calcination temperature on the hydrophilicity of TiO_2 films prepared by the sol-gel method," *Applied Surface Science*, vol. 462, pp. 480–488, 2018.

[52] D. Wei, Y. Zhou, and C. Yang, "Yang, Structure, cell response and biomimetic apatite induction of gradient TiO_2-based/nano-scale hydrophilic amorphous titanium oxide containing Ca composite coatings before and after crystallization," *Colloids and Surfaces B: Biointerfaces*, vol. 74, no. 1, pp. 230–237, 2009.

[53] M. Sarraf, E. Zalnezhad, A. R. Bushroa, A. M. S. Hamouda, A. R. Rafieerad, and B. Nasiri-Tabrizi, "Effect of microstructural evolution on wettability and tribological behavior of TiO_2 nanotubular arrays coated on Ti–6Al–4V," *Ceramics International*, vol. 41, no. 6, pp. 7952–7962, 2015.

[54] Y. Luo, Y. Jiang, J. Zhu, J. Tu, and S. Jiao, "Surface treatment functionalization of sodium hydroxide onto 3D printed porous Ti6Al4V for improved biological activities and osteogenic potencies," *Journal of Materials Research and Technology*, vol. 9, no. 6, pp. 13661–13670, 2020.